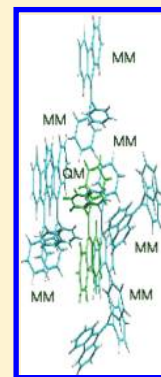


Quantum Chemistry Study on Internal Conversion of Diphenyldibenzofulvene in Solid Phase

Ming-Chung Li,^{†,‡} Michitoshi Hayashi,^{*,§} and Sheng-Hsien Lin^{⊥,||}[†]Department of Chemistry, National Tsing Hua University, Hsinchu 30013, Taiwan[‡]Molecular Science and Technology Program, Taiwan International Graduate Program, Academia Sinica, Taipei 115, Taiwan[§]Center for Condensed Matter Sciences, National Taiwan University, Taipei 106, Taiwan, Republic of China[⊥]Institute of Atomic and Molecular Sciences, Academia Sinica, Taipei, Taiwan 10617, Republic of China^{||}Department of Applied Chemistry, National Chiao Tung University, Hsinchu, Taiwan 30010, Republic of China Supporting Information

ABSTRACT: We investigate the nonradiative decay process of diphenyldibenzofulvene (DPDBF) in solid phase by using the quantum chemistry methods. To carry out the nonradiative rate constant calculation, we construct a solid phase model based on the ONIOM method. The geometry of the DPDBF molecule is optimized for the ground state by DFT and the first excited state by TD-DFT, and the corresponding vibrational frequencies and normal coordinates are computed. Under displaced–distorted harmonic oscillator potential approximation, Huang–Rhys factors are obtained. Vibronic coupling constants are calculated as a function of the normal mode based on Domcke’s scheme. We find that vibronic coupling constants of 12 modes with large reorganization energies are of similar order, and if this result is still valid for other modes, the internal conversion rate would be determined by high frequency modes because they have a significant nuclear factor that is related to Franck–Condon overlap integrals. We also find that geometrical changes are suppressed due to the stacking effect, which yields small Huang–Rhys values in the solid phase.



I. INTRODUCTION

Many organic materials are highly luminescent in their dilute solutions but weakly emissive when concentrated to the solid phases. The descending luminescence intensity in solid phase is believed to be a result of the formation of less emissive species such as delocalized excitons and excimers.¹ Therefore, concentration or aggregation quenching is a spiny problem in the development of photovoltaic cells,² optical lasers,³ organic light emitting diodes (OLEDs),^{4,5} etc., because most organic materials in these applications are used as solid thin films. To reach high emission efficiency in the solid phase, doping fluorescent molecules into the emitting layers is the most effective approach, but the fabrication process would become complicated and require more cost of production as well. In 2001, Tang et al. reported an uncommon phenomenon in which 1,1-substituted 2,3,4,5-tetraphenylsilole derivatives are strongly emissive in the solid phase; i.e., aggregation induced emission (AIE) was observed.⁶

This phenomenon provides a new way to solve the aggregation quenching problem because of the inherent favorable property. Since then, some other compounds with the same character have been reported as well; for example, diphenyldistyrylbenzenes, triphenylbenzenes, *N,N*-bis(salicylidene)-*p*-phenylenediamine, 1-cyano-*trans*-1,2-bis(4-methylphenyl)ethylene (CN-MBE), *cis*-2,5-diphenyl-1,4-distyrylbenzene (DPDSB), *cis,cis*-1,2,3,4-tetraphenylbutadiene (TPBD),^{7–14} etc.

AIE molecules are faintly emissive in solution phase but strongly luminescent in solid phase. It has been reported that for 1,1-disubstituted 2,3,4,5-tetraphenylsiloles, the radiative rate constants between solution and solid phase are slightly different.¹⁵ Therefore, the nonradiative process should play an important role in their luminescent characteristics. We notice that for AIE molecules, fluorescence quantum yield varies between two phases (solution and solid). Shuai et al. have reported a quantum chemistry calculation scheme of nonradiative rate constant in solution phase, and they have concluded that the Duschinsky rotation effect (DRE) is important for the case in which geometry changes drastically.^{16,17} However, no quantum chemistry modeling has so far been made for nonradiative rate constant in the solid phase, and thus it should be studied. DPDBF has been shown experimentally to be AIE active.¹⁸ In this article, we focus on the nonradiative process of DPDBF in the solid phase. To this end, we model DPDBF in the solid phase by using the ONIOM method.^{19–21} For a simple comparison, we also model DPDBF in solution phase by introducing a solvent model. This paper is organized as follows. In section II, the essence of theoretical treatments of internal conversion transition is briefly introduced.

Received: August 25, 2011

Revised: October 28, 2011

Published: November 03, 2011

In sections III and IV, computational details and analysis of the calculated data, including the calculation of Huang–Rhys factors, vibronic couplings, and nonradiative rate constants, are discussed. The conclusions are briefed in section V.

II. THEORETICAL BACKGROUND

A. Internal Conversion. The internal conversion is provided by the breakdown of the Born–Oppenheimer approximation via the nuclear kinetic energy operator.^{22–28} Applying the Born–Oppenheimer coupling Hamiltonian^{22,29–33} under displaced–distorted harmonic potential surface and making use of $n = 1/(e^{it(\omega' - \omega'') + (\hbar\omega')/(kT)} - 1)$ leads to the transition rate constant from the vibronic manifold $\{bv'\}$ to $\{av''\}$

$$W_{b \rightarrow a}^{nr} = \frac{1}{\hbar^2} \sum_l^{N'} |R_l^{ab}|^2 \int_{-\infty}^{\infty} dt \exp(it\omega_{ab}) K_l \prod_{j \neq l}^N G_j \quad (1)$$

where N is the number of the normal modes i , N' is the number of the normal modes i for which $R_l^{ab} \equiv -\hbar^2 \langle \Phi_a | (\partial \Phi_b) / (\partial Q_l) \rangle$ is not equal to zero, ω_{ab} is the energy difference between two electronic states, ω_i is the harmonic vibrational frequency of the mode i , and $(d' - d'')$ is displacement of the vibrational coordinate between the two electronic states. Introducing $g_j^\pm = (n+1)e^{it\omega''} \pm n \cdot e^{-it\omega''}$ and $f_j^\pm = 1 \pm ((\omega'' - \omega')/(\omega' + \omega''))g_j^\pm$ to K_l and G_j in eq 1 yields

$$G_j = \frac{2n(e^{\hbar\omega_j'/kT} - 1)e^{it(\omega_j' - \omega_j'')/2}}{(\omega_j' + \omega_j'')} \sqrt{\frac{\omega_j' \omega_j''}{f_j^- f_j^+}} \times \exp\left(\frac{-\omega_j' \omega_j'' (d' - d'')^2 (1 + 2n) - g_j^+}{\hbar(\omega_j' + \omega_j'')} \frac{1}{f_j^-}\right) \quad (2)$$

and

$$K_l = G_l K_l^0 \quad (3)$$

Here K_l^0 in eq 3 can be given by

$$K_l^0 = \frac{\omega_l' \omega_l''}{\hbar(\omega_l' + \omega_l'')} \frac{-(1 + 2n) \left(\frac{\omega_l'' - \omega_l'}{\omega_l'' + \omega_l'} \right) g_l^- + g_l^+}{f_l^- f_l^+} + \left[\frac{\omega_l' \omega_l'' (d' - d'')^2}{\hbar(\omega_l' + \omega_l'')} \right]^2 \left[\frac{(1 + 2n) - g_l^+}{f_l^-} \right]^2 \quad (4)$$

The single and double primes in eqs 2–4 denote vibrational frequencies belonging to the initial and final electronic states, respectively. To evaluate internal conversion rate constant efficiently, it is useful to rewrite eq 1 as

$$W_{b \rightarrow a}^{nr} = \frac{1}{\hbar^2} \sum_l^{N'} |R_l^{ab}|^2 \cdot F_l(\omega) \quad (5)$$

where

$$F_l(\omega) = \int_{-\infty}^{\infty} dt \exp(it\omega_{ab}) K_l^0 \prod_j^N G_j$$

B. Vibronic Coupling Constant. The electronic states can be treated in a perturbative manner, which gives the electronic wave functions as^{28,29,34}

$$\begin{aligned} \Phi_a(Q) &= \Phi_a^0(0) + \sum_{n \neq a} a_{an}(Q) \Phi_n^0(0) \\ &= \Phi_a^0(0) + \sum_{n \neq a} \frac{H'_{na}}{E_a^0(0) - E_n^0(0)} \Phi_n^0(0) \end{aligned} \quad (6)$$

and

$$\begin{aligned} \Phi_b(Q) &= \Phi_b^0(0) + \sum_{n \neq b} a_{bn}(Q) \Phi_n^0(0) \\ &= \Phi_b^0(0) + \sum_{n \neq b} \frac{H'_{nb}}{E_b^0(0) - E_n^0(0)} \Phi_n^0(0) \end{aligned} \quad (7)$$

where E_n^0 is the energy eigenvalue of the electronic wave function $\Phi_n^0(0)$, and the vibronic-coupling matrix element is

$$\begin{aligned} H'_{nk} &= \left\langle \Phi_n^0 \left| \sum_i \left(\frac{\partial V}{\partial Q_i} \right)_0 Q_i \right| \Phi_k^0 \right\rangle \\ &= \sum_i \left\langle \Phi_n^0 \left| \left(\frac{\partial V}{\partial Q_i} \right)_0 \right| \Phi_k^0 \right\rangle Q_i \equiv \sum_i \Lambda_i^{nk} Q_i \end{aligned} \quad (8)$$

Here in eqs 6–8, V and Q_i refer to the electrostatic potential and the vibrational normal coordinate of mode i , respectively, and the subscript and superscript 0 indicate the geometry at the ground state equilibrium.

Substituting eq 6 and eq 7 into $R_l^{ab} \equiv -\hbar^2 \langle \Phi_a | (\partial \Phi_b) / (\partial Q_l) \rangle$ and only considering two electronic states (ground and first excited) for DPDBF yields

$$\begin{aligned} R_l^{01} &= -\hbar^2 \left\langle \Phi_0(Q) \left| \frac{\partial}{\partial Q_l} \right| \Phi_1(Q) \right\rangle \\ &= -\hbar^2 (c_l^{01}) \end{aligned} \quad (9)$$

where the orthonormal property of electronic wave function $\Phi_n^0(0)$ has been used. The perturbative expansion coefficients concerning the ground and first excited states, c_l^{01} , can be written explicitly as

$$\begin{aligned} a_{10} &= \frac{H_{01}'}{E_1^0(0) - E_0^0(0)} = \frac{\langle \Phi_0^0 | (\partial V / \partial Q_l)_0 Q_l | \Phi_1^0 \rangle}{E_1^0(0) - E_0^0(0)} \\ &= \frac{\Lambda_l^{01} Q_l}{\Delta E_{01}} = c_l^{01} Q_l \end{aligned} \quad (10)$$

and l indicates the promoting mode.

III. COMPUTATIONAL DETAILS

To model the solid phase as well as to minimize the system size, we build a model based on the experimental crystal structure.¹⁸ The model consists of one centered DPDBF molecule with the six nearest neighbor molecules as shown in Figure 2. The ground and first excited states of the single DPDBF molecule with surrounding ones are computed by the ONIOM approach.^{19–21} In our ONIOM calculation, the system consists of two regions that are typically referred to as “layers”. The surrounding molecules are treated as a low layer in which inexpensive model chemistry

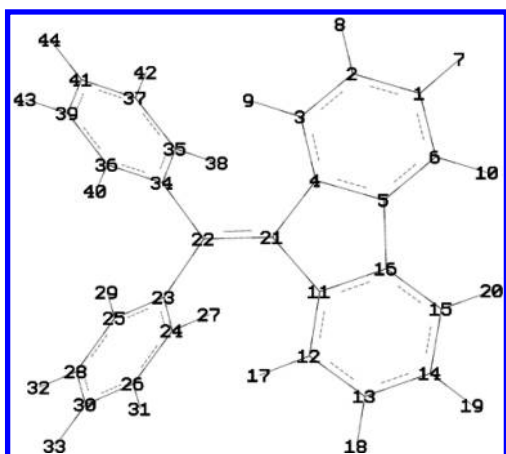


Figure 1. Chemical structure of diphenyldibenzofulvene (DPDBF).

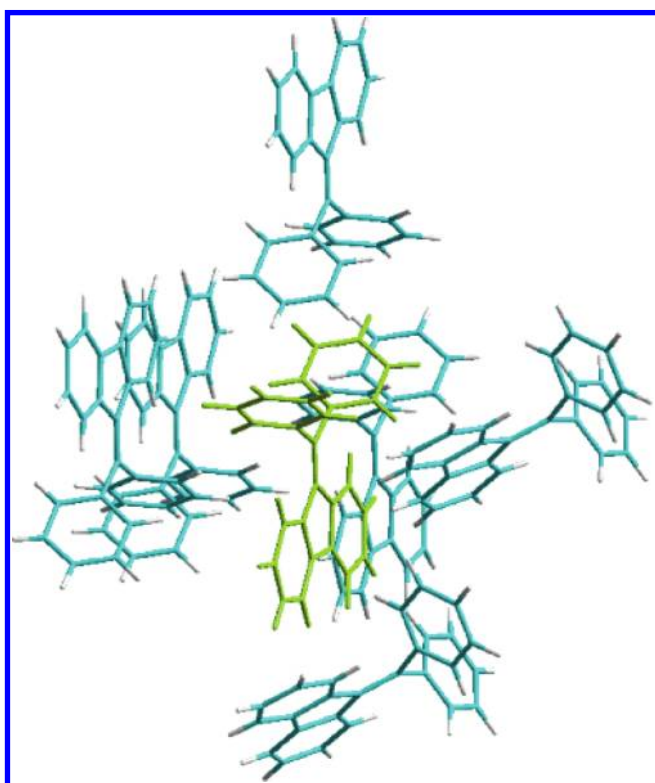


Figure 2. Solid phase model. Single centered DPDBF molecule with the six nearest surrounding molecules is depicted.

methods are applied. The inside molecule (i.e., excluding the surrounding ones) is treated as a high layer and calculated by more accurate methods. For the ground state, the chemical structures and vibrational frequencies of the high layer molecule are computed by density functional theory (DFT) with the B3LYP functional, and the low layer molecules are computed by molecular mechanics (MM) with UFF forces field. As for the first excited state, the chemical structures and vibrational frequencies of the high layer molecule are obtained at the TD-B3LYP level, and the excited state energy gradient is calculated numerically. The low layer molecules are also modeled by MM with UFF forces field. Note that in the optimization process, the surrounding molecules are kept frozen and only the inside

Table 1. Calculated Excitation Energies and Oscillator Strength of Single DPDBF Molecule in Solid Phase Model

absorption		
solid phase	excitation energy	f (oscillator strength)
excited state 1	3.469 eV (357.40 nm)	0.0084
excited state 2	3.949 eV (313.98 nm)	0.3407
expt. ^a	323 nm	
emission		
solid phase	excitation energy	f (oscillator strength)
excited state 1	2.727 eV (454.63 nm)	0.0144
expt. ^a	462 nm	

^a Reference 18.

molecule is optimized; i.e., “frozen optimization” is assumed. As for the solution phase, a single DPDBF molecule is placed in a cavity with the presence of a solvent (acetonitrile) and the polarizable continuum model (PCM) is adopted as the solvent model. The ground and first excited states of a single DPDBF in the solution phase model are computed at DFT and TD-DFT both with the B3LYP level, respectively.

To compute the vibronic coupling constant, Λ_i^{01} , the ground (first excited) state potential energy surface of a single DPDBF molecule along promotional modes is built at DFT (TDDFT). The ground state potential energy surface along two dihedral angles, C21–C22–C23–C24 and C21–C22–C34–C35 (see the geometry shown in Figure 1), is constructed at the DFT-(B3LYP) level. All the computations were performed at the 6-31G(d) basis set by using the Gaussian 09 package.³⁵ For internal conversion rate constant calculation, eqs 2–5 are coded in FORTRAN.

We optimize the geometries of the ground and first excited states of the centered DPDBF in solid phase model and calculate the excitation energies, oscillator strength, and vibrational normal modes. These calculated molecular properties are summarized in Table 1. Table 1 shows that the TD-DFT excitation energies are comparable with the experimental values. We find that the oscillator strength of the vertical transition from the ground to first excited states is 0.0084 and the ground to second excited states is 0.3407, which indicates that the first excited state is a dark state for absorption. We also find that the oscillator strength from the first to ground states is 0.0144, which is nearly two times larger than the one from the ground to first excited states. The transition energy between the first and second excited states is simply 0.48 eV. Thus, there are at least two possible pathways for the fluorescence decay, i.e., (i) direct radiative decay from the second excited to ground states and (ii) slow radiative decay from the first excited to ground states because of small oscillator strength (0.0144). It is not clear which pathway (or even other pathways) is dominant. However, we shall pay our attention to pathway (ii) (i.e., molecular emission is from the lowest excited state according to Kasha’s rule) in this article.

IV. RESULTS AND DISCUSSION

A. Huang–Rhys Factors. The Huang–Rhys (HR) factors (S_i and S_i') are computed by using $S_i = \omega_i'' q_i^2 / 2\hbar^{36}$ and $S_i' = \omega_i' \omega_i'' q_i^2 / (\omega_i' + \omega_i'')\hbar$, respectively, where ω_i and single and

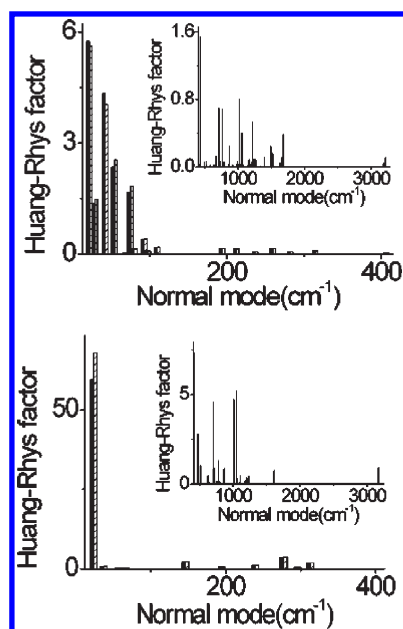


Figure 3. Calculated Huang–Rhys factors (S in black column and S' in sparse line column) of single DPDBF molecule in solid phase model (top) and in solution phase model (bottom). The calculations are performed using DFT and TDDFT at B3LYP levels with the 6-31G(d) basis set. In each panel, the inset is the wider energy range ($400\text{--}3000\text{ cm}^{-1}$) of the normal modes.

Table 2. Bond Lengths and Torsion Angles of the Ground^a and First Excited States^b for DPDBF in Solution Phase and Solid Phase

structure parameter ^c	solution phase	
	ground state	first excited state
C22–C23	1.491	1.445
C21–C22–C23–C24	55.72	22.49
C22–C34	1.491	1.445
C21–C22–C34–C35	55.49	22.49
C21–C22	1.369	1.471
C11–C21–C22–C23	18.46	61.19
C4–C21–C22–C34	18.54	61.19
structure parameter ^c	solid phase	
	ground state	first excited state
C22–C23	1.494	1.488
C21–C22–C23–C24	74.25	67.70
C22–C34	1.497	1.488
C21–C22–C34–C35	80.07	73.71
C21–C22	1.358	1.425
C11–C21–C22–C23	1.28	7.96
C4–C21–C22–C34	3.17	12.54

^a Calculated by DFT. ^b Calculated by TDDFT. ^c Bond lengths are in angstroms and torsion angles are in degrees.

double primes have the same definitions as in the theoretical section and q_i is the displacement of the “mass-weighted” vibrational coordinate between the two electronic states. We note that

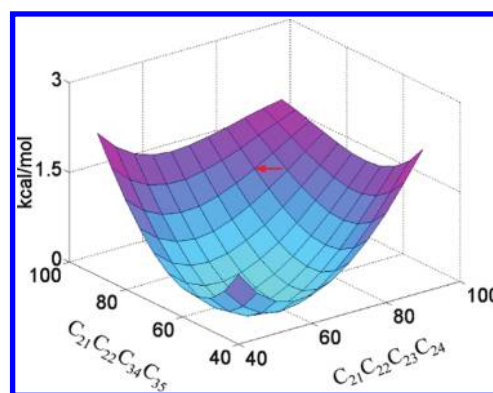


Figure 4. Ground state potential energy surface of DPDBF along two torsion angles C21–C22–C23–C24 and C21–C22–C34–C35 calculated using DFT at the B3LYP level with the 6-31G(d) basis set.

S_i will be equal to S_i' when the vibrational frequencies of the initial and final state are the same (i.e., $\omega_i' = \omega_i''$). The calculated HR factors are shown in Figure 3. We find that HR factors in solid phase are much smaller than those in solution phase, especially for the low frequency regions ($<100\text{ cm}^{-1}$). Mode analysis shows that low frequency ($<100\text{ cm}^{-1}$) modes belong to intramolecular rotation motions (phenyl rings rotation). Table 2 lists the calculated structure parameters for DPDBF in solution phase and solid phase by DFT/TDDFT (B3LYP), respectively. Larger geometry displacements can be found in solution phase. For example, in solution phase, the torsion angles C21–C22–C23–C24 and C21–C22–C34–C35 are (55.72° , 55.49°) and (22.49° , 22.49°) in the optimized structures of the ground and first excited states, respectively. Therefore, there are almost 33° differences between the ground and first excited state structures. This indicates a more planar structure is adopted in the excited state, which is rational because a planar structure can extend the conjugated length and make it stable. However, in solid phase, the torsion angles are already twisted, (74.25° , 80.07°), in the ground state. It becomes very difficult for the excited state geometry to be a planar structure because of the hindrance from neighboring molecules. In fact, the torsion angles in the excited state are (67.70° , 73.71°), and therefore the differences between ground and excited state structures are merely about 6° .

As shown in Figure 3, the HR factors in solution phase are much larger than those in solid phase. The smaller HR factors in the solid phase could result from the already twisted structure in the ground state. The ground state PES of single DPDBF molecule along C21–C22–C23–C24 and C21–C22–C34–C35 is drawn in the Figure 4. The minimum energy is taken as the reference zero point. There are obvious variations in torsion angles ($+20^\circ\sim 25^\circ$) in the ground state structure from solution to solid phase. It can be seen that the torsion angles variation due to the difference between the solution and solid phases gives rise to energy rising $+1.5\text{ kcal/mol}$. It indicates that a more twisted structure (74.25° , 80.07°) is not favorable in solid phase. However, this result contradicts the experimental fact because a more twisted structure was adopted in the solid phase.¹⁸ Therefore there should exist a “compensation” energy that makes the rising energy fall down. The compensation energy could be due to the intermolecular interaction (C–H... π interaction). It is a difficult task, however, to quantitatively evaluate the intermolecular interaction of DPDBF because it is known that the methods that take the electron correlation into account, for example, second-order

Table 3. Selected Promoting Modes of DPDBF in Solid Phase Model, Their Frequencies in the Ground and Excited States, Mode Assignments, Huang–Rhys Factors (S_i , S'_i), $F_i(\omega)$ Ratio ^a, and Reorganization Energies ^b

mode	ground state $\omega_i(\text{cm}^{-1})$	first excited state $\omega_i(\text{cm}^{-1})$	mode description ^c		S_i	S'_i	λ_i (cm^{-1})	$F_i(\omega)$ ratio
1	22.22	21.09	ring motion	the six member rings connected	5.756	5.606	118.25	1
2	29.30	34.16		to C22 atom	1.369	1.474	50.36	1.619
3	42.63	37.14			4.335	4.037	149.93	1.760
5	54.47	63.60			2.358	2.541	161.61	3.015
8	75.43	90.69			1.673	1.827	165.69	4.299
26 ^d	432.51	432.67	breathing	six member ring	1.542	1.543	667.61	20.512
39	665.82	643.77		six member ring	0.133	0.131	84.33	30.520
41 ^d	711.60	692.89		five member ring	0.703	0.694	480.86	32.848
43	723.11	722.69	CH out of plane wag	C24H27, C26H31, C30H33,	0.073	0.073	52.76	34.261
				C28H32, C25H29				
45 ^d	764.11	753.37		C28H32, C30H33, C26H31, C39H43,	0.688	0.683	514.55	35.716
				C41H44, C37H42				
53 ^d	868.57	866.11		C24H27, C26H31, C30H33,	0.245	0.245	212.20	41.061
54	870.75	870.09		C28H32, C25H29, C36H40, C37H42	0.134	0.134	116.59	41.25
65	989.58	989.73		CH of all six member rings	0.068	0.068	67.30	46.921
69 ^d	1022.72	1011.93	CCC bend	C36C39C41	0.810	0.806	815.62	47.974
71 ^d	1061.42	1026.70		CH bend	C39H43, C37H42, C26H31, C28H32	0.403	0.396	406.57
79	1166.57	1162.58		C1H7, C6H10, C14H19, C15H20	0.090	0.089	103.47	55.116
83	1207.88	1205.69		C12H17, C13H18, C14H19, C15H20,	0.053	0.053	63.90	57.159
				C3H9, C2H8				
84 ^d	1215.79	1212.28		C36H40, C39H43, C35H38, C37H42	0.536	0.536	649.78	57.472
87	1241.29	1239.29		C12H17, C13H18, C15H20, C2H8	0.098	0.098	121.45	58.752
88	1268.76	1280.87		C3H9, C6H10, C12H17, C15H20	0.093	0.093	119.12	60.724
97	1399.57	1406.09		C13H18, C14H19, C2H8, C1H7	0.122	0.122	171.54	66.660
100 ^d	1494.09	1486.70		C12H17, C13H18, C14H19, C15H20,	0.246	0.246	365.73	70.482
102 ^d	1522.77	1504.41		C3H9, C2H8, C1H7, C6H10	0.165	0.164	246.72	71.321
106	1631.73	1541.06	CC stretch	C1C2, C5C4	0.043	0.042	64.72	73.059
110	1652.92	1618.74		C2C3, C5C6, C12C13, C15C16	0.113	0.111	179.68	76.741
113	1661.67	1652.01		C36C39, C35C37, C24C26, C25C28	0.053	0.053	87.56	78.319
114 ^d	1678.29	1670.38		C21C22	0.388	0.388	648.11	79.190
117 ^d	3186.70	3182.61	CH stretch	C37H42, C35H38	0.042	0.042	133.67	150.881
126 ^d	3216.13	3217.62		C36H40, C39H43	0.115	0.115	370.03	152.540

^a Take a ratio to the minimal $F_i(\omega)$. ^b Selected reorganization >50 cm^{-1} . ^c With largest amplitude. ^d With large reorganization energy.

Møller–Plesset perturbation (MP2) and coupled cluster calculations (CCSD(T)), can extract the attraction energy between molecules, but these methods are both expensive approaches. Instead, we provide an alternative approach to estimating the intermolecular interaction of DPDBF dimer. We shall make an approximation that single DPDBF molecule roughly consists of four benzene molecules and one ethylene. From the crystal structure of DPDBF dimer,¹⁸ the intermolecular interaction of DPDBF dimer is, therefore, estimated in the following way: $\Delta E_{\text{vdw}}^{\text{DPDBFdimer}} \approx 4 \times \Delta E_{\text{vdw}}^{\text{benzenedimer}} + 1 \times \Delta E_{\text{vdw}}^{\text{ethylenedimer}}$. Evaluating the intermolecular interaction of benzene and ethylene dimer is much easier than DPDBF dimer. According to Tanabe's calculation,³⁷ the attraction energies of benzene and ethylene dimer are about -2.0 and -1.0 kcal/mol at the CCSD(T) level, respectively. The attraction energy of dimer DPDBF molecules, therefore, is about -9 kcal/mol, which is enough to compensate the rising energy ($+1.5$ kcal/mol). Our results show that although a more twisted structure is not favorable for an isolated molecule, it becomes favorable

through the intermolecular interaction (C–H... π interaction) in solid phase.

B. Vibronic Coupling Constant. Vibronic coupling (VC) constants as well as HR factors are crucial to evaluate the non-radiative rate constants. Although VC constants can be determined by ab initio calculation,³⁴ it would be a very expensive computation for large systems to evaluate the VC constants. Instead, for the sake of efficiency, we use the Domcke's method.^{38–40} A model Hamiltonian is formulated on a diabatic electronic basis

$$V = \frac{1}{2} \omega Q^2 \mathbf{I} + \begin{pmatrix} 0 & \Lambda_{01} Q \\ \Lambda_{01} Q & \Delta E_{01} + \gamma Q^2 \end{pmatrix} \quad (11)$$

and VC parameter (Λ_{01}) is estimated by fitting the ab initio PES function. Here $Q = (\omega/\hbar)^{1/2} q$ is the dimensionless normal coordinate and ΔE_{01} is the vertical excitation energy from ground to first excited state.

To demonstrate accuracy of this approach, we calculate the VC parameters (Λ_{12}) for formaldehyde by both ab initio calculation

Table 4. Parameters (in eV) Λ_{01} , γ , ω ; Vertical Excitation Energy (in eV) ΔE_{01} , and Vibronic Coupling Coefficient, c_i^{01} (dimensionless)

	solid phase					
	mode 26 ^a	mode 41 ^a	mode 45 ^a	mode 53 ^a	mode 69 ^a	mode 71 ^a
$(\Lambda_{01})^2$	0.094	0.040	0.092	0.068	0.037	0.021
γ	-0.028	-0.0137	-0.026	-0.020	-0.011	-0.006
ω	0.053	0.088	0.093	0.111	0.125	0.133
ΔE_{01}	3.469	3.469	3.469	3.469	3.469	3.469
c_i^{01}	0.088	0.058	0.087	0.075	0.056	0.041
	mode 84 ^a	mode 100 ^a	mode 102 ^a	mode 114 ^a	mode 117 ^a	mode 126 ^a
$(\Lambda_{01})^2$	0.066	0.047	0.071	0.040	0.022	0.031
γ	-0.020	-0.018	-0.024	-0.010	-0.007	-0.009
ω	0.156	0.1849	0.189	0.213	0.399	0.402
ΔE_{01}	3.469	3.469	3.469	3.469	3.469	3.469
c_i^{01}	0.074	0.063	0.077	0.058	0.043	0.051

^a See Table 3 for the mode assignment.

and Domcke's method (see Tables S1 and S2 in the Supporting Information). The fitting scheme clearly shows a distinctively large difference between the coupling constants of the symmetry allowed and those of the symmetry forbidden transitions. The fitting scheme for the zero coupling modes (i.e., the modes with vanished coupling matrix element $\langle \Phi_1(Q) | (\partial/\partial Q_i) | \Phi_2(Q) \rangle = 0$) yields nearly zero coupling values while for the nonzero coupling mode, the fitting scheme calculates the same order values of the ones obtained by the ab initio calculation.

Equation 5 clearly shows that the magnitude of the rate is determined by $R_i^{01} = -\hbar^2(c_i^{01})$ and $F_i(\omega)$. Suppose that one mode has a stronger coupling with an electronic transition or a larger $F_i(\omega)$; then, one can expect that the nonradiative rate will be fast. For the highly symmetry system, the coupling matrix element $\langle \Phi_0(Q) | (\partial/\partial Q_i) | \Phi_1(Q) \rangle$ will go away for modes $i \neq l$ (l : promotion mode); therefore, it is easy to examine which mode can be a promotion mode or not. However, the symmetry of the single DPDBF molecule in the solid phase model is C_1 due to the inhomogeneous environment so that all vibronic transitions are all symmetry allowed (i.e., $\Gamma(\langle \Phi_0(Q) | \partial/\partial Q_i | \Phi_1(Q) \rangle) = A$ for all modes i). Thus, there is not a way to judge whether a mode can be a promotion mode from its symmetry. Nevertheless, we note that for conjugated molecules, the carbon double bond stretching mode is usually assigned as the promotion mode because of a large reorganization energy, $\lambda_i = S_i\omega_i\hbar$.^{15,16} To examine this idea, we first group all the vibrational normal modes by their motions and only show the modes with the corresponding reorganization energies being larger than 50 cm^{-1} in Table 3. We then calculate the corresponding $F_i(\omega)$ and take a ratio with the minimal one (i.e., $F_1(\omega)$). We should note that in our calculation for the DPDBF case, there is not only one mode with large reorganization energy. For example, it can be seen that the modes with the three largest reorganization energies are mode 69 (CCC bend, 815.62 cm^{-1}), mode 26 (breathing, 667.61 cm^{-1}), and mode 84 (CH bend, 649.78 cm^{-1}). It is trivial to calculate VC parameters by Domcke's method for all modes. We only calculate 12 of them, which are mode 26, mode 41, mode 45, mode 53, mode 69, mode 71, mode 84, mode 100, mode 102, mode 114, mode 117, and mode 126, as shown in Table 3. These modes have a large reorganization energy and/or

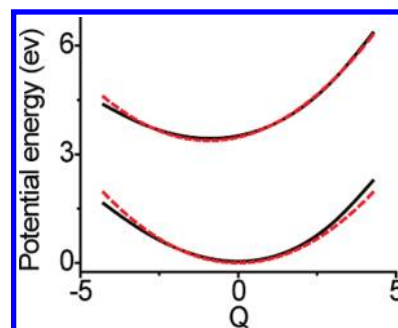


Figure 5. Calculated potential energy surfaces of the ground and first excited states along the CC double bond stretching mode in the solid phase model (1678.29 cm^{-1}). The calculations are performed by TDDFT at B3LYP levels with the 6-31G(d) basis set. The dashed curves show the corresponding PES function constructed from fitting data.

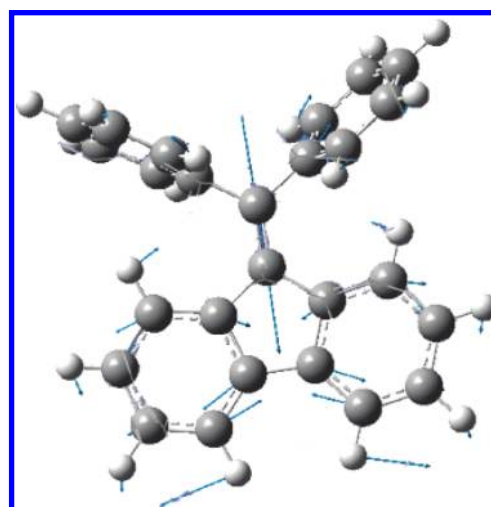


Figure 6. Schematic representation of the normal mode displacement vectors of mode 114 (CC double bond stretch 1678.29 cm^{-1}).

a large $F_i(\omega)$ value. We proceed to calculate PESs of the single DPDBF molecule along these modes and use the upper eigenvalue of the diabatic potential matrix of eq 11 to fit the PES of the first excited state. The fitting parameters (Λ_{01} , γ) are summarized in Table 4. The corresponding PES constructed from fitting data and the normal mode displacements for mode 114 (CC double bond stretch) as an example are shown in Figure 5 and Figure 6, respectively.

With the fitting parameter Λ_{01} and the vertical excitation energy ΔE_{01} , the vibronic coupling coefficient c_i^{01} can be obtained by eq 10. The vibronic coupling coefficient for 12 modes is summarized in Table 4. We find that there are no positive correlations between reorganization energies and vibronic coupling coefficients within our present data; i.e., larger reorganization energies do not indicate larger vibronic coupling coefficients. For example, the largest reorganization energy is 815.62 cm^{-1} for mode 69, but the largest vibronic coupling coefficient is 0.088 for mode 26. However, we do find that there are positive correlations between $F_i(\omega)$ and the promoting mode frequency, i.e., the larger mode frequency, the larger $F_i(\omega)$, and this relation is effective for all modes. The largest $F_i(\omega)$ for DPDBF, therefore, is for mode 126 (CH stretch). The calculated nonradiative rate constant is $3.816 \times 10^{10} \text{ s}^{-1}$ if the mode 126 (CH stretch) is

chosen as a promotion mode. In a similar way, we can also calculate the nonradiative rate constants from the second excited state to the ground state (see Supporting Information, Table S3). The mode 126 (CH stretch) is chosen as a promotion mode, and the calculated nonradiative rate is $3.429 \times 10^{10} \text{ s}^{-1}$, which is of the same order of magnitude as that from the first excited state to the ground state. For the solution phase, our calculation (Figure 3) shows that the HR factors are much larger than the ones in the solid phase model because the geometry indeed changes drastically in the solution phase model. In other words, DRE should be important, and the nonradiative rate constant calculation in solution phase should take into account DRE.^{16,17,24,41} Shuai et al. have reported a calculation scheme of nonradiative rate constant in solution phase. In this study, we show that it is possible to perform the nonradiative rate constant calculation in solid phase.

V. CONCLUSION

We have modeled a single molecule in its solid phase environment by using the ONIOM method. It is worthy to mention that our modeling way is a general approach since, by ONIOM method, solid phase environments can be easily modeled for other systems. According to eqs 2–5, the nonradiative rate constant is determined by three molecular properties: (1) the vibrational frequencies of the electronic ground and excited states, (2) Huang–Rhys factors, and (3) vibronic coupling constants. Our calculations show that for the solid phase model, the magnitude of $F_I(\omega)$ is proportional to the promotion mode frequency, and thus the largest $F_I(\omega)$ is for mode 126 (CH stretch).

From the ground state potential energy surface of a single, isolated molecule along the torsion angles C21–C22–C23–C24 and C21–C22–C34–C35, the stable structure shows (55.72° , 55.49°). On the other hand, in the presence of the intermolecular interaction (C–H... π interaction) in solid phase, a twisted structure (74.25° , 80.07°) becomes favorable. This more twisted structure is similar to the structure of the first electronic excited state. Therefore, Huang–Rhys factors become smaller compared with those in the solution phase model.

It is noted that there are some conditions in our solid phase modeling: (i) only the minimal intermolecular interactions are taken into account. However, to meet a real situation, we should increase the number of molecules as many as possible; (ii) “the frozen optimization” is assumed. In general, there will not only be one molecule to be excited when a light or laser shines on the sample. Therefore, we should allow more molecules to be involved in electronic excitation. Nevertheless, we carry out our investigation under these conditions in this study as the first step to model a nonradiative process of molecules in solid phase.

■ ASSOCIATED CONTENT

Supporting Information. Calculated potential energy surfaces of formaldehyde (Figure S1); calculated potential energy surfaces and Huang–Rhys factors for second excited state of single DPDBF molecule in solid phase model (Figure S2 and S3); nonadiabatic coupling matrix element and fitting parameters of formaldehyde (Table S1 and S2); fitting parameters for second excited state of single DPDBF molecule in solid phase model (Table S3). This material is available free of charge via the Internet at <http://pubs.acs.org>.

■ AUTHOR INFORMATION

Corresponding Author

*E-mail: atmyh@ntu.edu.tw.

■ ACKNOWLEDGMENT

This work is supported by National Science Council (99-2628-M-002-009).

■ REFERENCES

- (1) Birks, J. B. In *Photophysics of Aromatic Molecules*; Wiley: London, U.K., 1970.
- (2) Tang, C. W. *Appl. Phys. Lett.* **1986**, *48*, 183–185.
- (3) Zeng, L.; Miller, E. W.; Pralle, A.; Isacoff, E. Y.; Chang, C. J. *J. Am. Chem. Soc.* **2006**, *128*, 10–11.
- (4) Tang, C. W.; VanSlyke, S. A. *Appl. Phys. Lett.* **1987**, *51*, 913–915.
- (5) Adachi, C.; Tsutsui, T.; Saito, S. *Appl. Phys. Lett.* **1990**, *57*, 531–533.
- (6) Luo, J.; Xie, Z.; Lam, J. W. Y.; Cheng, L.; Chen, H.; Qiu, C.; Kwok, H. S.; Zhan, X.; Liu, Y.; Zhu, D.; et al. *Chem. Commun.* **2001**, 1740–1741.
- (7) An, B. K.; Kwon, S. K.; Jung, S. D.; Park, S. Y. *J. Am. Chem. Soc.* **2002**, *124*, 14410–14415.
- (8) Chen, J.; Xu, B.; Ouyang, X.; Tang, B. Z.; Cao, Y. *J. Phys. Chem. A* **2004**, *108*, 7522–7526.
- (9) Jayanty, S.; Radhakrishnan, T. P. *Chem.—Eur. J.* **2004**, *10*, 791–797.
- (10) Li, S.; He, L.; Xiong, F.; Li, Y.; Yang, G. *J. Phys. Chem. B* **2004**, *108*, 10887–10892.
- (11) Tracy, H. J.; Mullin, J. L.; Klooster, W. T.; Martin, J. A.; Haug, J.; Wallace, S.; Rudloe, L.; Watts, K. *Inorg. Chem.* **2005**, *44*, 2003–2011.
- (12) Bhongale, C. J.; Chang, C. W.; Lee, C. S.; Diau, E. W. G.; Hsu, C. S. *J. Phys. Chem. B* **2005**, *109*, 13472–13482.
- (13) Toal, S. J.; Jones, K. A.; Magde, D.; Troglor, W. C. *J. Am. Chem. Soc.* **2005**, *127*, 11661–11665.
- (14) Xie, Z.; Yang, B.; Cheng, G.; Liu, L.; He, F.; Shen, F.; Ma, Y.; Liu, S. *Chem. Mater.* **2005**, *17*, 1287–1289.
- (15) Yu, G.; Yin, S.; Liu, Y.; Chen, J.; Xu, X.; Sun, X.; Ma, D.; Zhan, X.; Peng, Q.; Shuai, Z.; Tang, B. Z.; Zhu, D.; Fang, W.; Luo, Y. *J. Am. Chem. Soc.* **2005**, *127*, 6335–6346.
- (16) Peng, Q.; Yi, Y.; Shuai, Z.; Shao, J. *J. Am. Chem. Soc.* **2007**, *129*, 9333–9339.
- (17) Peng, Q.; Yi, Y.; Shuai, Z. *J. Chem. Phys.* **2007**, *126*, 114304–114313.
- (18) Tong, H.; Dong, Y.; Hong, Y.; Häussler, M.; Lam, J. W. Y.; Sung, H. H. Y.; Yu, X.; Sun, J.; Williams, I. D.; Kwok, H. S.; et al. *J. Phys. Chem. C* **2007**, *111*, 2287–2294.
- (19) Dapprich, S.; Komáromi, I.; Byun, K. S.; Morokuma, K.; Frisch, M. J. *J. Mol. Struct. (Theochem)* **1999**, *461*, 1–21.
- (20) Vreven, T.; Morokuma, K.; Farkas, Ö.; Schlegel, H. B.; Frisch, M. J. *J. Comput. Chem.* **2003**, *24*, 760–769.
- (21) Torrent, M.; Vreven, T.; Musaev, D. G.; Morokuma, K.; Farkas, Ö.; Schlegel, H. B. *J. Am. Chem. Soc.* **2002**, *124*, 192–193.
- (22) Lin, S. H. *J. Chem. Phys.* **1966**, *44*, 3759–3767.
- (23) Lin, S. H.; Fujimura, Y.; Neusser, H. J.; Schlag, E. W. *Multi-photon Spectroscopy of Molecules*; Academic: New York, 1984; Chapter 2.
- (24) Mebel, M.; Hayashi, M.; Liang, K. K.; Lin, S. H. *J. Phys. Chem. A* **1999**, *103*, 10674–10690.
- (25) Liang, K. K.; Chang, R.; Hayashi, M.; Lin, S. H. *Principle of Molecular Spectroscopy and Photochemistry*; National Chung Hsing University Press: Taichung, China, 2001; Chapters 2 and 5.
- (26) Shiu, Y. J.; Hayashi, M.; Mebel, A. M.; Chen, Y. T.; Lin, S. H. *J. Chem. Phys.* **2001**, *115*, 4080–4094.
- (27) Yeung, E. S.; Moore, C. B. *J. Chem. Phys.* **1974**, *60*, 2139–2147.
- (28) Lin, S. H.; Eyring, H. *Proc. Natl. Acad. Sci. U.S.A.* **1974**, *71*, 3415–3417.

- (29) Lin, S. H. *Proc. R. Soc. London A* **1976**, *352*, 57–71.
- (30) Mebel, A. M.; Chen, Y. T.; Lin, S. H. *Chem. Phys. Lett.* **1996**, *258*, 53–62.
- (31) Hayashi, M.; Mebel, A. M.; Liang, K. K.; Lin, S. H. *J. Chem. Phys.* **1998**, *108*, 2044–2055.
- (32) Chin, H.; Shiu, Y. J.; Wang, H. W.; Chen, Y. L.; Wang, C. C.; Lin, S. H.; Hayashi, M. *J. Chin. Chem. Soc.* **2006**, *53*, 131–152.
- (33) Mebel, A. M.; Hayashi, M.; Lin, S. H. *Chem. Phys. Lett.* **1997**, *274*, 281–292.
- (34) Lin, C. K.; Li, M. C.; Yamaki, M.; Hayashi, M.; Lin, S. H. *Phys. Chem. Chem. Phys.* **2010**, *12*, 11432–11444.
- (35) Frisch, M. J.; Trucks, G. W.; Schlegel, H. B.; Scuseria, G. E.; Robb, M. A.; Cheeseman, J. R.; Scalmani, G.; Barone, V.; Mennucci, B.; Petersson, G. A.; et al. *Gaussian 09*, revision A.02; Gaussian, Inc.: Wallingford CT, 2009.
- (36) Lin, S. H.; Chang, C. H.; Liang, K. K.; Chang, R.; Shiu, Y. J.; Zhang, J. M.; Yang, T. S.; Hayashi, M.; Hsu, F. C. *Adv. Chem. Phys.* **2002**, *121*, 1–88.
- (37) Tsuzuki, S.; Honda, K.; Uchimaru, T.; Mikami, M.; Tanabe, K. *J. Am. Chem. Soc.* **2002**, *124*, 104–112.
- (38) Seidner, L.; Stock, G.; Sobolewski, A. L.; Domcke, W. *J. Chem. Phys.* **1992**, *96*, 5298–5309.
- (39) Woywod, C.; Domcke, W.; Sobolewski, A. L.; Werner, H. J. *J. Chem. Phys.* **1994**, *100*, 1400–1413.
- (40) Domcke, W.; Köppel, H.; Cederbaum, L. S. *Mol. Phys.* **1981**, *43*, 851–875.
- (41) Hayashi, M.; Mebel, A. M.; Liang, K. K.; Lin, S. H. *J. Chem. Phys.* **1998**, *108*, 2044–2055.